Deposition of Lithium on a Plasma Edge Probe in TFTR
- Behavior of Lithium-Painted Walls Interacting with Edge Plasmas -

Y. Hirooka[1)], K. Ashida[2)], H. Kugel[3)], D. Walsh[4)], W. Wampler[4)],
M. Bell[3)], R. Conn[1)], M. Hara[2)], S. Luckhardt[1)], M. Matsuyama[2)],
D. Mansfield[3)], D. Mueller[3)], C. Skinner[3)], T. Walters[3)], and K. Watanabe[2)]

[1)]University of California, San Diego, 9500 Gilman Dr. , La Jolla, CA92093-0417, USA.
[2)]Toyama University, Gofuku 3190, Toyama 930, Japan
[3)]Princeton University, P. O. Box 451, Princeton, NJ08543, USA
[4)]Sandia National Laboratories, Albuquerque, NM87185-5800, USA

Corresponding author: Y. Hirooka
Phone number: 619-534-9720
Fax number: 619-534-7716
e-mail address: yhirooka@fusion.ucsd.edu
Key words: TFTR, lithium, lithium-pellet injection, wall conditioning, impurity deposition, codeposition, mixed material

ABSTRACT

Recent observations have indicated that lithium pellet injection wall conditioning plays an important role in achieving the enhanced supershot regime in TFTR. However, little is understood about the behavior of lithium-coated limiter walls, interacting with edge plasmas. In the final campaign of TFTR, a cylindrical carbon fiber composite probe was inserted into the boundary plasma region and exposed to ohmically-heated deuterium discharges with lithium pellet injection. The ion-drift side probe surface exhibits a sign of codeposition of lithium, carbon, oxygen, and deuterium, whereas the electron side essentially indicates high-temperature erosion. It is found that lithium is incorporated in these codeposits in the form of oxide at the concentration of a few percent. In the electron side, lithium has been found to penetrate deeply into the probe material, presumably via rapid diffusion through interplane spaces in the graphite crystalline. Though it is not conclusive, materials mixing in the carbon and lithium system appears to be a key process in successful lithium wall conditioning.

1. Introduction

DISCLAIMER

It is widely recognized that wall conditioning is essential in achieving high-performance plasma confinement in a magnetic fusion device. To review recent achievements in fusion research, one cannot ignore the roles wall conditioning has played. These include the supershot mode in TFTR by helium discharge conditioning [1], the VH-mode in DIII-D by the combination of boronization and helium conditioning [2], and most recently the enhanced-supershot mode in pre-boronized TFTR by lithium pellet injection [3]. Among all the wall conditioning techniques applied in TFTR, lithium conditioning is the only one with which the energy confinement time has significantly been increased [4].

To interpret briefly these wall conditioning effects, helium discharge conditioning depletes the plasma-interactive walls of previously implanted fuel particles, which then results in reduced edge recycling in the following shots. Boronized walls have been found to capture large amount of fuel particles as well as impurities [5]. It immediately follows from these arguments that the combination of boronization and helium conditioning can provide further improvement. However, the effect of lithium pellet injection has not yet been well interpreted to date.

The effect of lithium pellet injection on the plasma performance in TFTR was first accidentally discovered in 1990 [3]. Since then much has been demonstrated about beneficial effects of lithium-coated first walls in TFTR [4]. In contrast, lithium injection has only brought modest improvement to other confinement devices, including DIII-D [6], JIPP-IIU [7], TdeV [8] and ALCATOR C-Mod [9]. First-order explanation is that all these devices run divertor discharges, meaning that by nature the effect of first walls is minimal, no matter how they are conditioned. Nevertheless, the question remains open as to how lithium-coated walls interact with edge plasmas.

In the meantime, plasma-facing materials mixing came up as a new issue in the fusion community with the advent of the ITER divertor cassette design in which beryllium, carbon and tungsten are employed for in-vessel components, positioned closely one another. However, this is not a specific issue of ITER. To the contrary, one finds a variety of materials mixing opportunities in other fusion devices as well, either in operation or under design. From this materials mixing point of view, TFTR provides a rather interesting opportunity, mixing of lithium with deuterium, tritium, and carbon from the underlying graphite tiles, together with other impurities such as oxygen.

In this work, a deposition probe positioned in the boundary region of TFTR has been exposed to fiducial deuterium-deuterium (D-D) discharges with lithium pellet injection in January, 1997. Extensive materials analysis has been done on this probe, using a variety of materials analysis techniques, to find out about spatial distributions and chemical states of mixed materials of lithium, tritium, deuterium, lithium, oxygen, carbon and other impurities. This paper is intended to report the essence of these materials analysis data and to discuss possible mechanisms, affecting the plasma interaction behavior with the lithium-coated first walls in TFTR. Comprehensive data sets obtained from these individual analysis techniques will be published separately [10, 11].

2. Experimental

The deposition probe used in this work is a machined piece of a C-C (carbon-carbon) composite material from FMI Inc. in the form of cylinder with the length of 9.1

cm and the diameter of 5.6 cm. This C-C composite material has a 4-dimensionally woven fiber structure and the impurity contents are listed in Table 1. On January 31st, 1997 in the final campaign of TFTR, 6 OH (ohmically-heated) discharge cleaning shots were done with helium. The probe was then inserted into the boundary region through the Bay-D port located at R = 2.624 m and exposed to OH D-D (deuterium-deuterium) discharges with lithium pellet injection.

In these three D-D shots, the discharge parameters are: plasma heating power of 1 MW; plasma current of 1.6 MA; edge safety factor of about 4; major radius of 2.6m and minor radius of 0.95m. The deposition probe is thus positioned 2.4 cm off the poloidal center of the plasma. As to the vertical position, in the minor radius direction, the probe top surface was set at about 2 cm off the last closed flux surface. The flattop duration was about 3 seconds during which lithium pellets were injected individually with some intervals in-between. The number of injected pellets are 2, 4 and 4, respectively, for these discharges. The pellet is in the form of cylinder with the length of about 2 mm and the diameter of about 2 mm, containing 3 mg of lithium (i.e., 3×10^{20} Li-atoms). Following these successful D-D discharges, the last one was disrupted right after the first pellet was injected. However, the disruption effect on the probe experiment is expected to be minimal because statistically in TFTR, the stored energy release is directed towards the bumper limiter. The total number of injected pellets was 11, meaning 3.3×10^{21} Li-atoms, which provides an average lithium coverage of 1 monolayer/cm^2 over the TFTR internal surface area. It is important to mention here that the injected lithium was enriched with Li-6 to 95.6% in this campaign to avoid resonance absorption of the RF heating power.

After it was extracted from the TFTR system, the probe was immediately subjected to smear tests for tritium monitoring to ensure the safety. The probe was then transported in an argon-purged container to Sandia National Labs. and NRA (nuclear reaction analysis) was performed on March 14th, 1997, using the X-IBA (external ion beam analysis) facility. For this analysis it is not necessary to section the probe, so that the elemental mapping of lithium and deuterium was performed over the entire surface. The nuclear reactions used in this analysis are: ^{7}Li(p, α)α and ^{3}He(d, p)α, the former of which means that the analysis was performed on the diluted lithium isotope.

The probe was then sent overseas to Toyama Univ. Hydrogen Isotope Res. Ctr. where tritium-compatible XPS (X-ray induced photoelectron spectroscopy) and SIMS (secondary ion mass spectrometry) are available. On July 2nd, 1997, the probe was cut into small specimens for a series of XPS-SIMS measurements. After this the probe was transported back to the UCSD-Fusion Lab. and surface morphology analysis with SEM (scanning electron microscopy) was conducted on December 4th, 1997. Due to the limited machine time on these material analysis facilities, as will be seen in the following sections, effort was concentrated on the comparison in surface characteristics between the ion drift side vs. electron drift side of the plasma-front surface of the probe.

3. Results and Discussion

3-1. Evaluation of edge plasma conditions

As to edge plasma parameters, there was unfortunately no direct measurements during the course of deposition probe experiments. However, relevant edge plasma data

are available from earlier measurements [12], using a reciprocating probe, conducted for the core plasma parameters similar to those employed in this work. The edge plasma density and temperature, selected for the probe position from this database, are about 2.5 x 10^{12} 1/cm^3 and 30 eV, respectively. Substituting these data into the sheath expressions for a floating surface in a collisionless plasma [13], the parallel energy flux density has been calculated to be about 260 W/ cm^2. Assuming the perpendicular to parallel heat flux ratio to be 0.05 - 0.5[14], the heat flux deposited on the probe top surface is 13 - 130 W/ cm^2. Taking into account the retained heat effect from previous discharges, the probe surface temperature is calculated to have reached 450 °C, 570 °C, 667 °C, and 579 °C, respectively, during the four lithium-pellet injected discharges for the deposition probe measurements [15].

3-2. Deposition probe materials analysis

3-2-1. Surface appearance and microscopic morphology analysis with SEM

The deposition probe after the plasma exposure in TFTR is shown in Fig. 1. Notice that there is clearly a difference in appearance between the electron and ion drift sides. Due to the machine configurations resulting in shadowing effects in some area, the heat deposition on the e-side is expected to be higher than that on the i-side for a limiter-like structure inserted from the Bay-D port. Consistent with this, the e-side surface appears to be burned and sooty, indicating high-temperature erosion, whereas the i-side suggests a rather mild erosion condition.

These macroscopic observations are compared with microscopic analysis with SEM. Shown in Figs. 2 (a)-(d) are the electron micrographs of the probe surfaces, perpendicular and parallel to the fiber bundle weaving direction. One finds strong surface modifications both on the e-side and i-side surfaces, compared with as-machined surfaces (not reported here due to the limited space). On the e-side perpendicular surface, shown in Fig. 2 (a), protruding nodular structures are observed. These are eroded fiber bundles with deeply etched boundaries, losing binder skins. Similar nodular structures have been observed in other tokamak experiments [16]. On the parallel surface in Fig. 2 (b), again, fiber bundles can be seen eroded and torn apart.

In contrast, scale-like structures are observed on the i-side surfaces, shown in Figs. 2 (c) and (d), indicative of incomplete film deposition. Discontinuous features such as these scales or islands are often observed at early stages of film deposition where the film thickness is not great enough to cover the initial surface roughness of the substrate. Because the probe was exposed to only a few discharges, the incompleteness of film coverage is highly possible.

Interestingly, the surface morphologies observed on the specimen on the outboard are similar to those on the e-side. Also, similarities are found between the inboard and i-side surfaces. These results indicate the particle (fuel and impurities) and heat flows, along with the magnetic field, crossing over the deposition probe at a characteristic angle. Corroborating this argument, the scale-structures on the i-side appear to wave in one direction. Further details on the particle transport is beyond the scope of this paper.

3-2-2. Deuterium and lithium mapping by NRA

Shown in Fig. 3 (a) are the results of NRA radial mapping of deuterium and lithium on the plasma-front surface as a function of distance from the outer edge. The probing depth in this analysis is about 1 μm. Notice that the i-side contains significantly larger amount of deuterium and lithium than the e-side, while these concentration profiles generally increase towards the center. This is believed to be related to the temperature differences between the i-side and e-side and also between the outer edge and center because the retention of hydrogenic species in carbonaceous materials is well known to decrease as temperature increases [17]. Because of its low melting point of 180.7 °C, resulting in a tendency of evaporation, the retention of lithium is expected to behave similarly to that of deuterium. In addition to the themal effect, codeposition is considered to have contributed to the increase in deuterium and lithium retention on the i-side.

The distribution profiles along the side wall in the minor radius direction are shown in Fig. 3 (b). Similarly to the plasma-front surface, considerably more deuterium and lithium are detected in the i-side than in the e-side. Again, this is due to the temperature and codeposition effects. Notice that these profiles intersect each other half way down to the bottom, which is presumably due to the recycling of previously implanted deuterium and lithium from the surrounding walls.

3-2-3. Elemental analysis with SIMS

Specimens cut from the e-side and i-side of the plasma-front surface of the probe were analyzed with both positive and negative ion SIMS, using an 5 keV argon ion beam as the probe beam. Shown in Figs. 4 (a) and (b) are the positive and negative SIMS spectra, respectively, both from the i-side specimen. Caution must be taken in interpreting these spectra because peak intensities are not necessarily proportional to elemental concentration on the surface.

In the positive SIMS data, shown in Fig. 4 (a), one finds most of the predictable elements and their isotopes, including hydrogen, lithium, carbon, together with some metallic impurities such as iron and chromium. In addition, sodium and potassium are detected at rather high intensities. Alkaline metals tend to generate high intensity peaks in positive SIMS, due to their low ionization potentials [18]. Also, as shown in Table 1, the C-C composite material used for the probe contains relatively large amount of ash impurities. Therefore, we do not consider that these alkaline impurities are from TFTR.

Concerning the details on SIMS data, both Li-6 and Li-7 are detected but the intensity ratio is about 10, a factor of about two off from the enrichment ratio in the injected lithium pellets. As pointed out in the previous section, this deviation is believed to be due to the contribution of recycling Li-7 from the first wall. Unlike other metal hydrides [19, 20], no clear peak is found either for LiH^+ or LiD^+. Lithium hydride is a line compound in the phase diagram and the solid solution is mostly in the liquid phase at temperatures above the lithium melting point [21]. As a result, lithium and hydrogenic

species are not strongly bound in the i-side codeposited materials. Instead of hydride, one finds several indications of oxides at M/e = 28 for $^6Li\ _2O^+$, 29 for $^6Li^7LiO^+$ and 30 for $^7Li\ _2O^+$, the chemistry of which will be discussed in the following section.

Interestingly, the peaks suggestive of CH^+, C_2H^+, CD^+ (or CH_2^+), and C_2D^+ (or $C_2H_2^+$), are seen in the spectra, indicating the bonding between carbon and hydrogen isotopes. This is quite consistent with the conjecture on codeposited materials of carbon and hydrogenic species. Also, detected are peaks suggestive of C^6Li^+, C^7Li^+, $C_2{}^6Li^+$, $C_2{}^7Li^+$, $C_3{}^6Li^+$, $C_3{}^7Li^+$, which may be from metastable intercalation compounds such as C_6Li or from the line compound carbide, αCLi [21]. Interestingly, these peaks are not seen in the e-side surface data (not reported here due to the limited space). Nonetheless, the question remains open as to in what form lithium exists in the codeposited materials.

Turning to negative SIMS data, shown in Fig. 4 (b), again, caution needs to be taken because several halogen elements are detected at high intensities, due to their high sensitivities to negative SIMS. For a similar reason to alkaline metals, we do not consider halogen peaks to be pertinent with TFTR plasmas. The detection of CH-, CD-compound ions supports the above-mentioned carbon hydride argument. Also, oxygen is believed to be a constituent of codeposited materials, as will be discussed in the XPS analysis, though part of it is due to air exposure.

To minimize the surface effect on SIMS data, depth profile data were taken. Shown in Fig. 5 (a) are the data on lithium, $^6Li^+$ normalized by $^{12}C^+$, down to the depth about 0.1 μm. In the time-to-depth conversion, the averaged atomic spacing of 6.69Å for the c-axis and 2.5Å for the a-axis is used because the probe material has a 4-dimensionally woven fiber bundle structure and the argon ion beam diameter (1 mm) is large enough to sputter bundles in all directions. Again, data indicate that the i-side contains more lithium than the e-side. Also, notice similarities between the e-side and outboard, and between the i-side and inboard surfaces. This is the same trend as that was observed in surface morphologies with SEM.

The e-side specimen was subjected to deeper profiling and the result is shown in Fig. 5 (b). Lithium, deuterium and oxygen are detected even at the depth exceeding 10 μm, at which depth the surface roughness effect is not quite important (see Fig. 3). As mentioned earlier, there was no direct surface temperature measurement on the probe. To evaluate these depth data, we assume that for simplicity, the e-side surface temperature was maintained at 1000K for 1 second. Due to the 4-dimensional structure, it is virtually impossible to find the exact literature data needed here. Nonetheless, the diffusivity of lithium in pyrolytic graphite, $D_{Li} = 3 \times 10^3 \exp(-1.83\ [eV]/kT)$ [22], reported for the basal plane direction is relevant because carbon hexagonal planes within an individual fiber are aligned in parallel. The characteristic diffusion length, given by $\sqrt{Dt}$ where D is diffusivity and t is time, has been calculated to be 13.4 μm which is of the same order as the SIMS depth data. As to deuterium penetration, the tritium diffusivity reported for a 3-dimensional C-C composite, $D_T = 1.72 \exp(-52.531\ [kJ/mol]/RT)$ [23], is used and the characteristic diffusion length has been calculated to be 5.56 μm. This must be corrected by the ratio of $\sqrt{m_T / m_D}$ to 6.81 μm. This is still a bit short falling to match the data. Considering the complexity, however, this discrepancy is not surprising. As for oxygen penetration, unfortunately, diffusivity data are not available under relevant conditions. There are two possibilities, however: the attachment of oxygen to the metastable lithium-

intercalated graphite structure and/or the formation of another intercalation compound such as C_8O_2OH [24]. Further discussion on this subject is beyond the scope of this work.

3-2-4. Surface chemistry analysis with XPS

In this section, the surface chemistry analysis with XPS is discussed. It is important to mention here to avoid confusion that compared with that by SIMS, the sensitivity of lithium detection by XPS is significantly smaller. In the following XPS data, therefore, lithium is not seen. Nonetheless, it is possible to investigate the chemistry of it from the valence electron binding energy analysis on other elements such as oxygen and carbon, having reasonably high sensitivities for O1s and C1s, respectively.

The results of binding energy analysis are shown in Figs. 6 (a)-(d). Oxygen is detected on the as-machined surface but at a significantly lower intensity, compared with that on the i-side surface. This is believed to be due to air exposure. Therefore, we consider that most oxygen detected on the e-side and i-side is from TFTR. For more detailed binding energy analysis, O1s peaks have been deconvoluted into component peaks, those of which shown in Fig. 6 (c) are taken from the i-side specimen. These component peaks are related to oxygen bound in the form of -OH, CO- and M_xO_y (metal-oxide). Correlated to the SIMS data, the most likely metal for the M_xO_y compound is lithium. From the areas below these peaks and wide energy range data [10], the concentration of lithium is estimated to be a few percent. This is significantly less than the averaged lithium coverage of 1 monolayer (see Section 2). However, considering the diffusion effects inward and perhaps outward as well, leading to materials mixing, this small concentration in the i-side codeposits is not totally surprising. Similar XPS analysis on the e-side specimen has resulted in even less lithium than this, which is consistent with the SIMS data (see Fig. 5 (a)) and also the NRA data (see Figs. 4 (a) and (b)).

Turning to carbon chemistry data, shown in Figs. 6 (b) and (d), the major component peak is due to carbon in the graphite crystalline, both for the as-machined and i-side specimens. The other peak, much pronounced on the i-side specimen, is believed to be due to carbon compounds in the form of $-CH_2-$, -CO and -COH. These are believed to illustrate the carbon chemistry in the codeposited materials although air exposure may have contributed to an extent. Not having a covalent bonding, no clear sign of C_6Li is seen in the XPS data. The corresponding peaks observed on the e-side are significantly smaller (data not reported here due to the limited space).

3-2-5. Spontaneous tritium release

The probe was subjected to on-site smear tests for tritium monitoring at PPPL. The total tritium content over the probe surface was estimated to be 30 μCi. However, it was requested in these tests that the plasma-interacted areas not be affected for the sake of subsequent materials analysis. The smear samples were thus taken from the bottom of the probe (see Fig. 1). This has led to the underestimation of tritium contents.

It has often been observed that graphite materials implanted with hydrogenic species decomposes in moist air even at room temperature but the rate decays rather rapidly [25]. Two months after plasma exposure, however, the probe radioactivity was found to be much higher than expected at the time when NRA was performed at SNL, penetrating a vinyl glovebox wall with a thickness of about 2 mm within a day or so.

Three months later at Toyama Univ., we observed significant tritium release upon opening the argon-packed container. Tritium release was even more pronounced, exceeding 10 pCi/cc in a glovebox, while the probe was sliced into small specimens for the SIMS-XPS analysis. Afterwards, further cuttings were done on these specimens in order that the amount of tritium was absolutely evaluated using the combustion method. Results are: 2.4 μCi/g in the e-side; 4.0 μCi/g in the i-side; 3.5 μCi/g in the outboard; and 11 μCi/g in the inboard [11]. From these data, one expects the total tritium content exceeding the initial on-site smear test data by orders of magnitude. Interestingly, however, tritium was not detected in thermal desorption measurements conducted for a specimen sectioned from the i-side side wall (see Fig. 3) up to about 900 °C [26]. This is primarily because the gas detection limit is 10^{-9} Torr and also because the noise level is relatively high due to the previous use with tritium-containing gases.

Four months later at UCSD during the course of SEM analysis, no tritium release was observed with the detection limit of 5 pCi/cc. Smear tests conducted along with facility decontamination have indicated that there is essentially no tritium contamination, other than the surfaces directly in contact with the specimens, inside as well as outside the vinyl glovebox. Although as such, radioactivity measurements have not always been quantitative in this work, our observations suggest that immediately after TFTR exposure the probe may have contained tritium of the order of 1 mCi and thus the radioactivity took almost a year to decay.

4. Summary and the hypothesis of lithium-conditioned wall mechanism

This work has presented the first set of materials analysis data on an edge probe exposed to TFTR plasmas with lithium pellet injection. The probe has been found to be deposited with particle and heat fluxes in the manner that shows the flow direction characterized by the magnetic configuration. The i-side surface exhibits a clear sign of codeposition of carbon, lithium, deuterium, oxygen, etc. whereas the e-side indicates high-temperature erosion. Despite its high reactivity to form various compounds, lithium has been detected only in the form of oxide in these codeposits. This solid-phase chemistry can perfectly be explained by the Gibb's free energy of formation argument in classical thermodynamics. However, we conjecture more non-equilibrium nature in the interaction of lithium-coated walls with edge plasma environment. The indications of metastable graphite intercalation compounds may be a reflection of this aspect.

In recent experiments related to materials mixing, carbon deposits have been observed to be mixed up with substrate beryllium, via outward diffusion, at elevated temperatures [27, 28]. One extrapolates from this that if the host material is lower-Z than deposits, diffusion can be outward as well as inward to mix materials. Carbon walls with lithium coatings provide an interesting opportunity for such materials mixing. Even if it is covered with arriving impurities, lithium may be able to penetrate deposits to create a new surface, as long as the wall temperature is high enough to drive diffusion mixing. When it

is sputtered, lithium is likely to be self-redeposited, not being able to overcome the sheath potential, due to its high efficiency of secondary ion formation [29]. This not only reduces erosion loss but maintains surface gettering.

Consistent with this hypothesis, enhanced supershots in TFTR require wall to be coated with lithium on the bumper limiter area, where the temperature is relatively high, rather than on the mid-plane the confinement plasma directly touches on [30]. This temperature effect partially explains recent observations that tokamaks running divertor discharges do not seem to benefit from lithium wall conditioning because plasma-interactive surface temperatures are claimed to be controlled as low as room temperature. As such, data are suggestive of the key mechanism of successful lithium wall conditioning. Unfortunately, however, we can not be any more conclusive than this due to the shutdown of TFTR.

Acknowledgment

This work is supported by the Princeton University Subcontract, the U.S. Dept. of Energy Grant, and also the Ministry of Education of Japan. Special thanks goes to the safety staff members, including B. Elkin at SNL and S. O'brien at UCSD.

Sandia is a multiprogram laboratory operated by Sandia Corporation, a Lockheed Martin Company, for the United States Department of Energy under contract DE-AC04-94AL85000.

References

[1] H. F. Dylla et al., J. Nucl. Mater. **162-164**(1989)128-137.
[2] G. L. Jackson et al., J. Vac. Sci. & Technol.-**A10**(1992)1244-1251.
[3] J. L. Terry et al. Proc. 13th Int. Conf. on Plasma Physics and Controlled Nuclear Fusion Research, Washington, USA, 1990, Paper: A-V-5.
[4] D. Mansfield et al. Phys. Plasmas **3**(1996)1.
[5] J. Winter et al., J. Nucl. Mater. **162-164**(1989)713-723.
[6] G. L. Jackson et al., J. Nucl. Mater. **241-243**(1997)655-659.
[7] H. Sugai et al., J. Nucl. Mater. **220-222**(1995)254-258.
[8] B. Terreault et al. J. Nucl. Mater. **220-222**(1995)1130-1134.
[9] J. L. Terry, "Lithium Wall Conditioning of Metal Walls in Alcator C-Mod", presented at the Workshop on Lithium Effects in Plasmas, Oct. 17-18th, 1996, Princeton, Workshop summary published in Nucl. Fusion **37**(1997)705-711.
[10] K. Ashida et al., "Surface Characterization of TFTR Graphite Probe by XPS-SIMS" Ann. Rep. of Hydrogen Isotope Res. Ctr., Toyama Univ., **17**(1997) in press.
[11] M. Hara et al. , "Analysis of Tritium Implanted in an Edge Probe in TFTR", ibid.
[12] C. S. Pitcher et al., Nucl. Fusion **32**(1992)239-256.
[13] P. C. Stangeby et al., Nucl. Fusion **32**(1992)2079-2089.
[14] P. C. Stangeby in "Physics of Plasma-Wall Interactions in Controlled Fusion", (ed.) D. E. Post and R. Behrisch, Plenum Press NATO ASI Series Vol. 131 (1984).
[15] H. S. Carslaw and J. C. Jaeger, "Conduction of Heat in Solids", Clarendon Press, (1959).
[16] Y. Hirooka and R. W. Conn in "Atomic and Plasma-Material Interaction Processes in Controlled Thermonuclear Fusion" (ed.) R. K. Janev and H. W. Drawin, Elsevier Scince (1993).
[17] R. A. Causey, J. Nucl. Mater. **162-164**(1989)151-161.
[18] C. A. Andersen and J. R. Hinthorne, Ana. Chem. **45**(1973)1421-1438.
[19] K. Ashida et al. J. Nucl. Mater. **210**(1994)233-238.
[20] Y. Hirooka et al., J. Nucl. Mater.**114**(1983)341-343.
[21] T. B. Massalski (ed.), "Binary Alloy Phase Diagrams (2nd ed.)" Vol. 2, ASM International (1990).
[22] B. Jungblut and E. Hinkis, Phys. Rev. **B40**(1989)10810-10815.
[23] S. Alberici et al., Fusion Technol. **28**(1995)1108-1113.
[24] F. A. Cotton and G. Wilkinson, "Advanced Inorganic Chemistry" 5th Ed. John Wiley & Sons, (1988).
[25] S. Chiu and A. A. Haasz, J. Vac. Sci. & Technol **A9**(1991)747-752.
[26] K. Ashida et al. "Surface Analysis of TFTR Graphite Probe and Thermal Desorption of Gases", presented at the Japanese Atomic Energy Society Meeting, Mar. 26-28th,1998, Osaka.
[27] Y. Hirooka et al., J. Nucl. Mater. **230**(1996)173-177.
[28] K. Ashida et al., Fusion Eng. & Design, Special Issue "Beryllium Studies for Fusion", Part-1, **37**(1997)307-315.
[29] A. Krauss et al., J. Nucl. Mater. **103&104**(1981)239-244.
[30] D. K. Mansfield et al. "Lithium Conditioning Experiments on TFTR: An Overview", presented at the same workshop as Ref. [9].

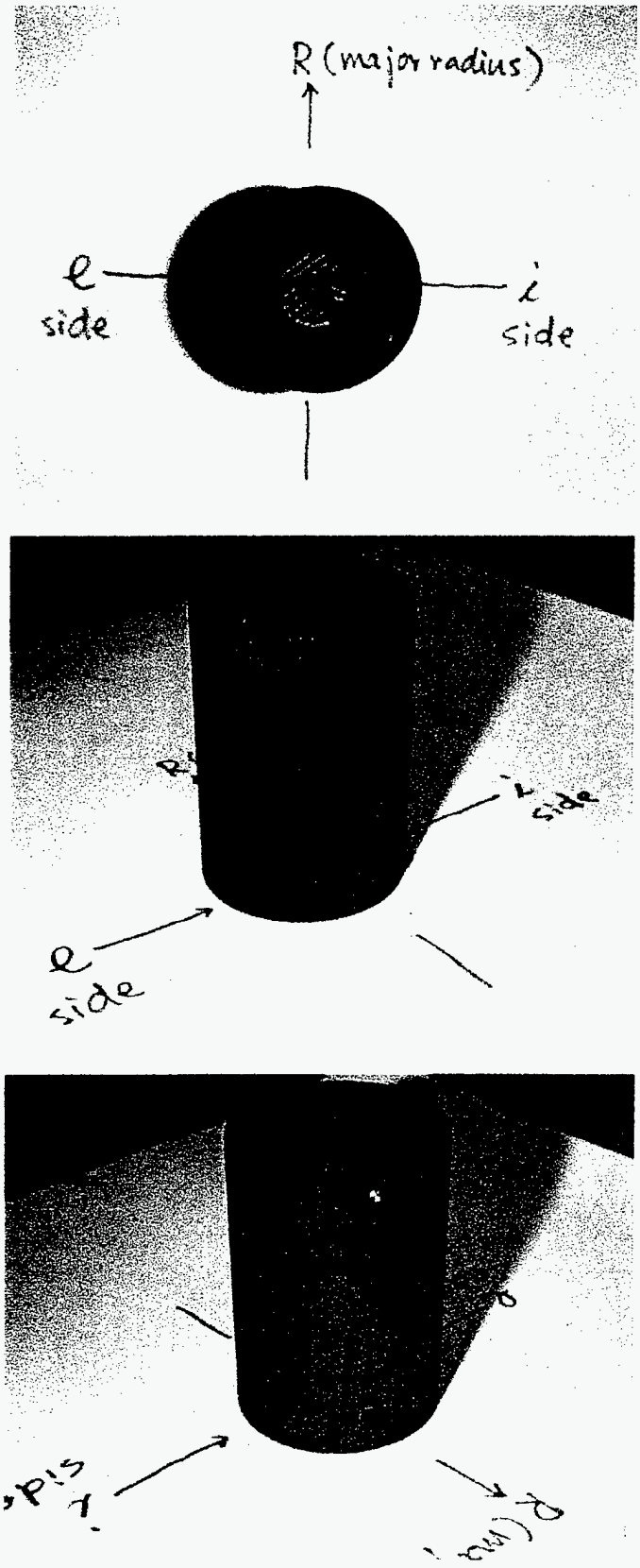

Fig. 1 The deposition probe after TFTR exposure.

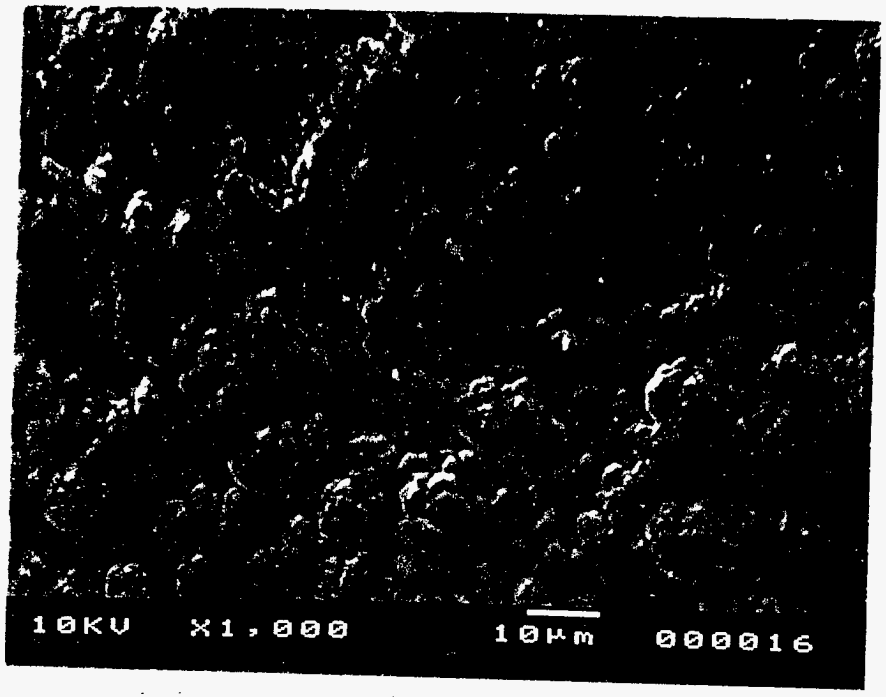

(a) e-side (⊥ fiber direction)

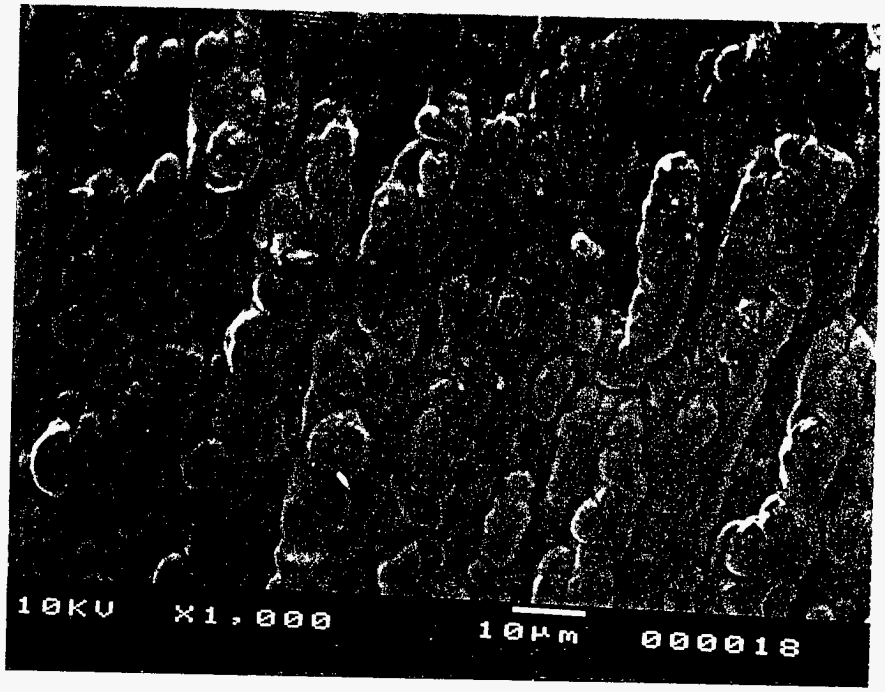

(c) e-side (// fiber direction)

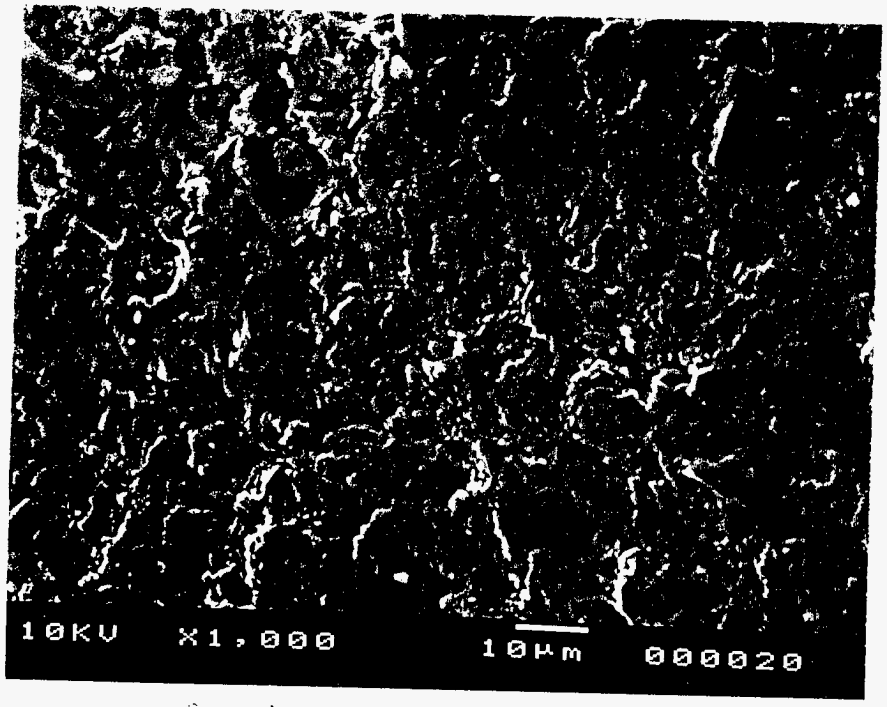

Fig. 2 (b) i-side (⊥ fiber direction)

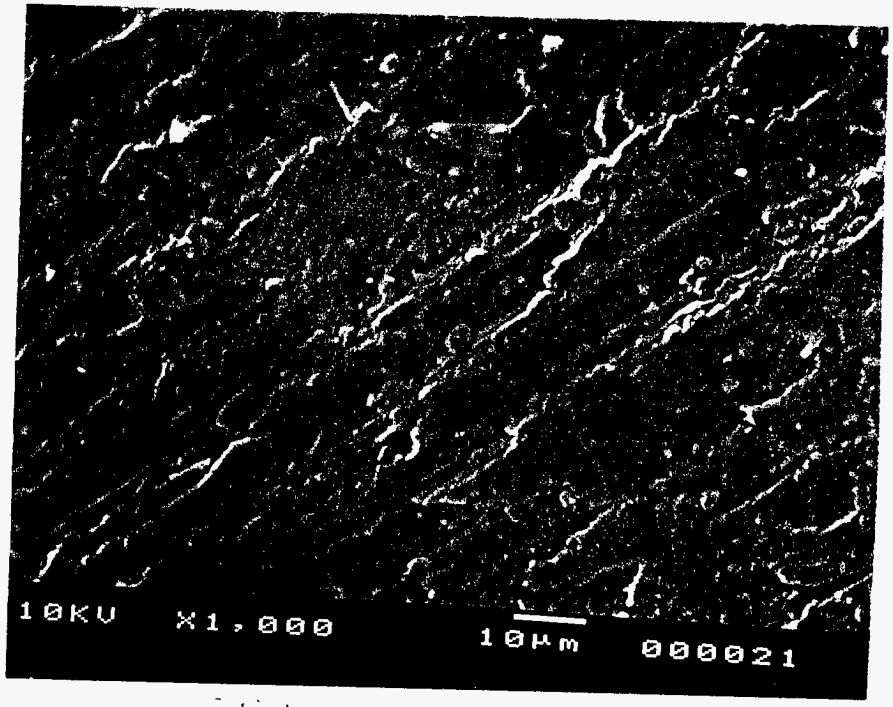

(d) i-side (// fiber direction)

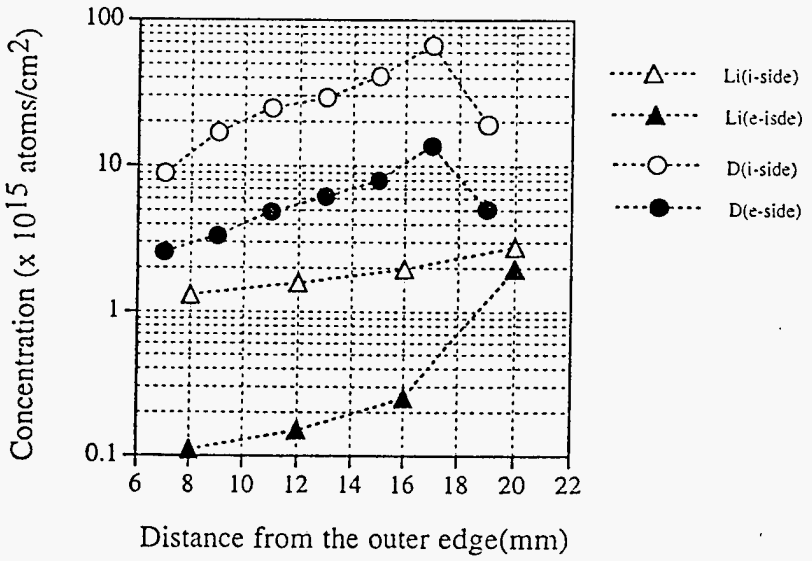

(a)

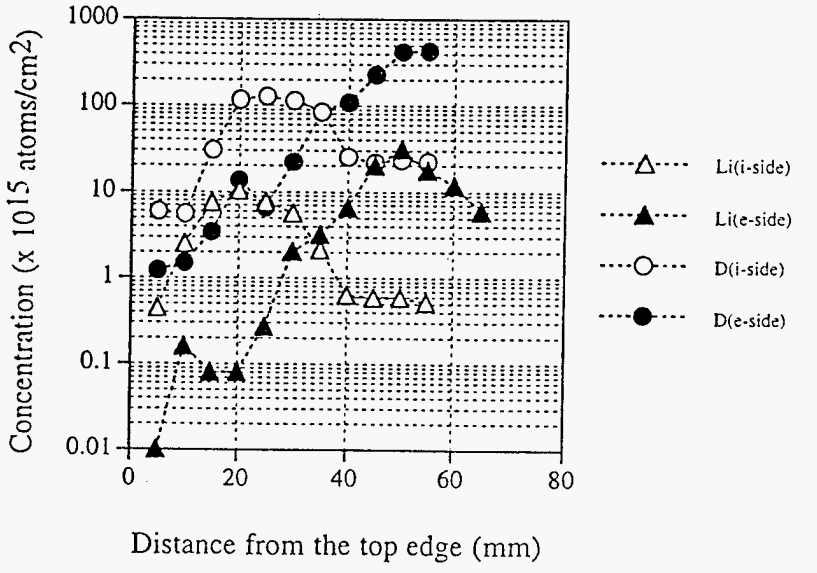

(b)

Fig. 3 Lithium (Li-7) and deuterium distribution profiles on (a) front surface and (b) side wall of the probe.

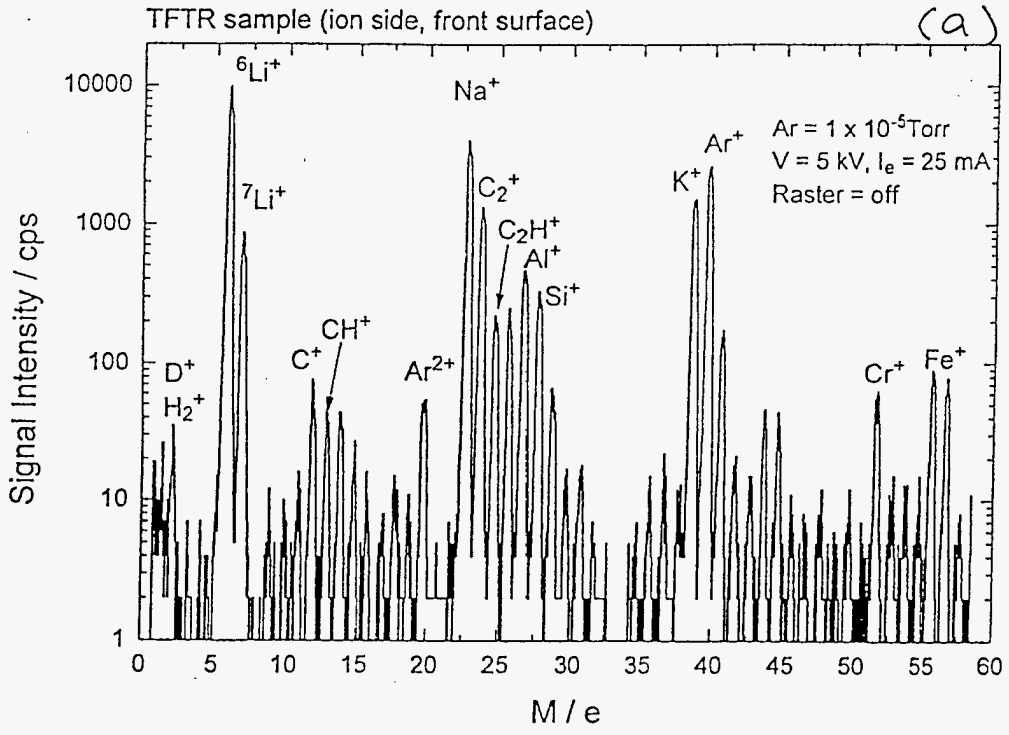

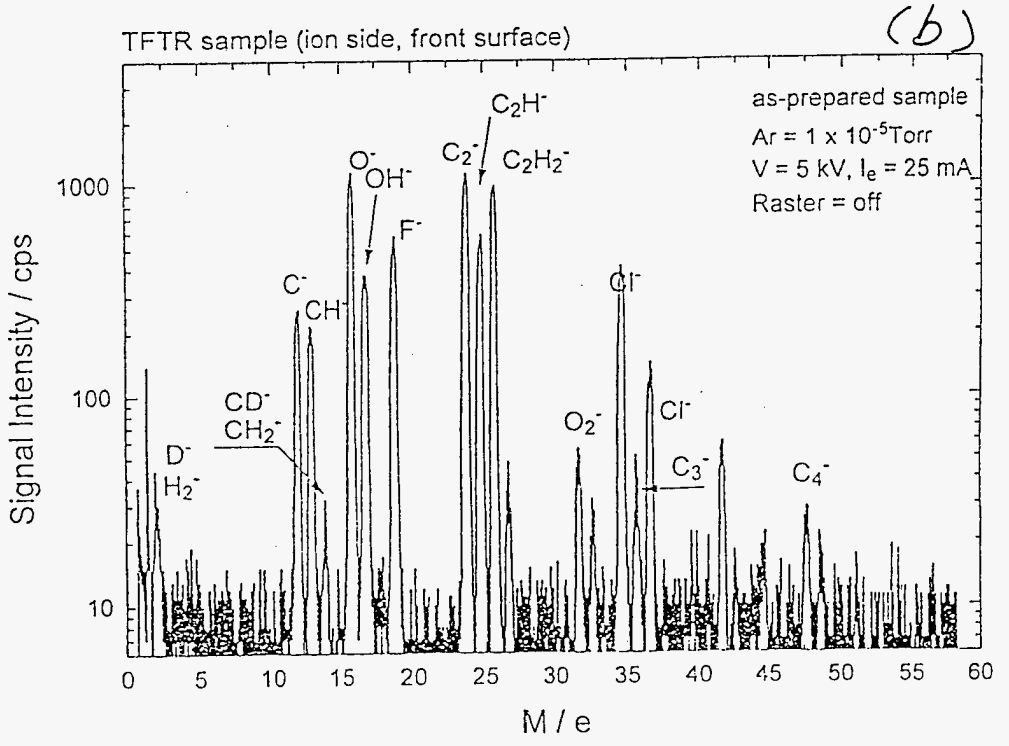

Fig. 4 SIMS analysis on the ion drift side surface: (a) positive ions and (b) negative ions.

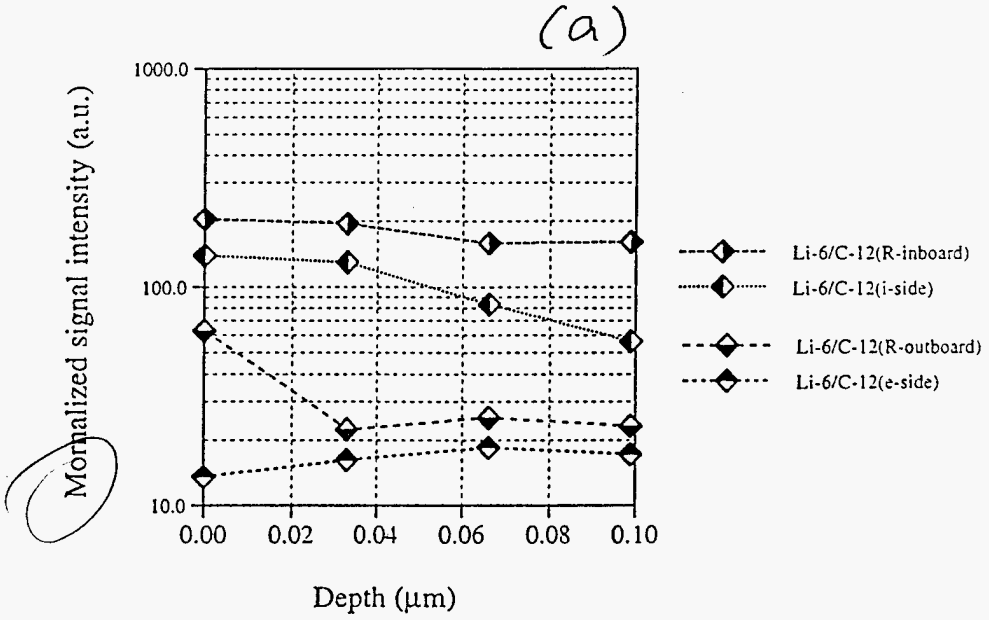

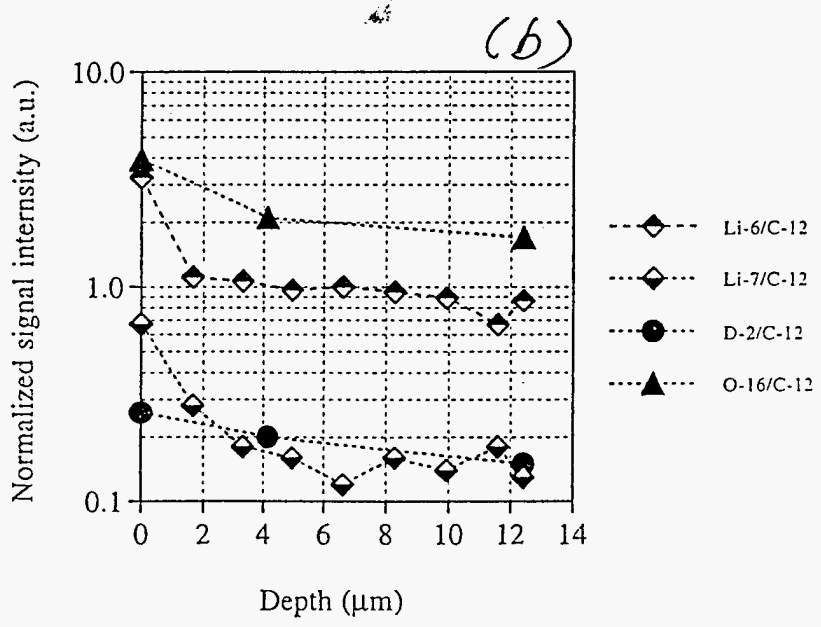

Fig. 5 SIMS depth profile data, normalized by C-12: (a) Li-6 profiles and (b) deeper profiles into the electron drift side surface.

d what distance from surface?
and comparison to Fig 3 NRA data

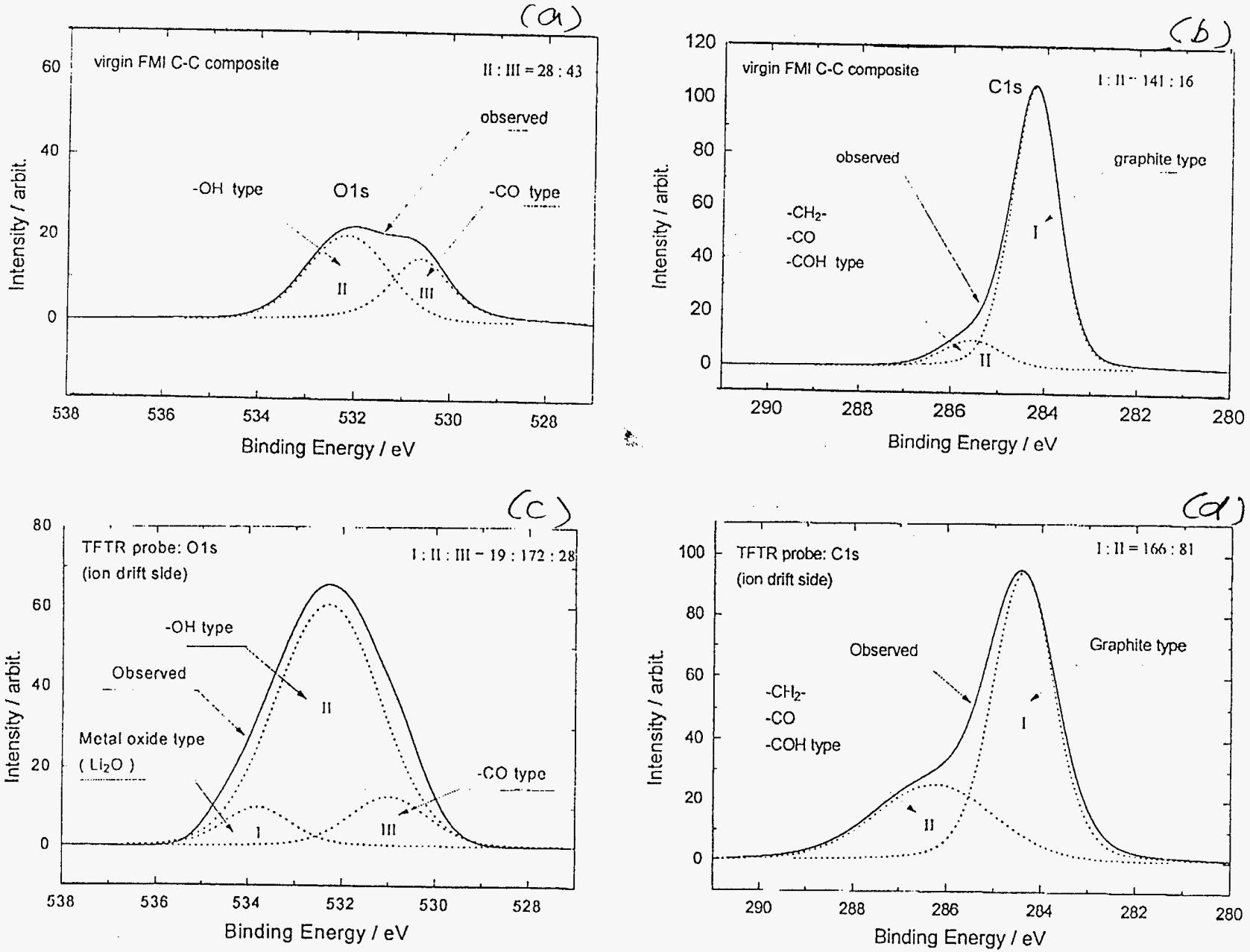

Fig. 6 Deconvoluted O1s and C1s peaks: (a), (b) from virgin sample, and (c), (d) from the ion drift side surface.

Report Number (14) SAND--98-1236C
CONF-980560--

Publ. Date (11) 199805
Sponsor Code (18) DOE/ER, XF
UC Category (19) UC-400, DOE/ER

DOE